Genome Biology

METHOD

Open Access

Leaf: an ultrafast filter for population-scale long-read SV detection

Chenxu Pan[1*] and Knut Reinert[1,2]

*Correspondence: chenxu.pan@fu-berlin.de

[1] Department of Mathematics and Computer Science, Freie Universität Berlin, Takustr. 9, 14195 Berlin, Germany
[2] Department of Computational Molecular Biology, Max Planck Institute for Molecular Genetics, Berlin 14195, Germany

Abstract

Advances in sequencing technology have facilitated population-scale long-read structural variant (SV) detection. Arguably, one of the main challenges in population-scale analysis is developing effective computational pipelines. Here, we present a new filter-based pipeline for population-scale long-read SV detection. It better captures SV signals at an early stage than conventional assembly-based or alignment-based pipelines. Assessments in this work suggest that the filter-based pipeline helps better resolve intra-read rearrangements. Moreover, it is also more computationally efficient than conventional pipelines and thus may facilitate population-scale long-read applications.

Keywords: Filter-based pipelines, Intra-read SV detection, Population-scale long-read applications, Generative model, Extended SAM/BAM

Background

Advancements in long-read sequencing have reached a level of accuracy and yield that allows population-scale applications [1]. Pacific Biosciences (PacBio) and Oxford Nanopore Technologies (ONT) are the two leading long-read sequencing platforms in the field. The PacBio platform can generate high fidelity (HiFi) reads, which are > 15 Kbps highly accurate reads [2]. The ONT platform can produce much longer reads (> 4 Mbps) at a lower cost, while the reads are less accurate [3]. Existing research has shown that long-read sequencing can discover a substantial proportion of previously undetected SVs [4–10]. Long-read sequencing research in recent years has provided insight into structural variants at a population level, such as the study of structural variants in the sequencing of 3622 Icelanders [11] and the Human Pangenome Project [12], which creates a more sophisticated and complete human reference genome of global genomic diversity. Long-read sequencing has also been applied to population-scale SV detection in fields like agriculture [14–15] and metagenomics [16, 17].

Ongoing advances in computational tools in the past years have facilitated long-read applications [18–20]. Alignment and de novo assembly are the main approaches for long-read sequencing analysis 21 [22–25]. Assembly-based approaches are commonly more effective in reconstructing highly diverse structures in sequences than alignment-based approaches [26, 27]. Nevertheless, de novo assembly requires higher read coverage and more computationally demanding [28], and thus it is challenging to apply assembly-based approaches to population-scale sequencing analysis [13, 14, 29, 30]. Population-scale analytical pipelines are supposed to be both effective and efficient [31, 32]. Although more advanced tools are constantly introduced in the rapidly developing areas [33–37]. Arguably, the main challenge in population-scale applications remains developing efficient and scalable analytical pipelines.

Here, we propose the filter-based pipeline for population-scale long-read SV detection. Different from conventional pipelines, such as assembly- or alignment-based ones, filter-based pipelines capture SV signals at a very early stage. Intuitively, it would be helpful to detect SV signals at an early stage because of the ultra-long read potentially containing intra-reads SVs that are likely missed by many existing assembly or alignment-based methods. To validate the feasibility of filter-based pipelines, we implemented Leaf (i.e., LinEAr Filter) within our long-read computational toolkit Linear. Assessments based on high-quality datasets and benchmark tools in this work suggest that filter-based pipelines are comparable to or outperform conventional pipelines in terms of detecting complex intra-read rearrangements and computational efficiency.

Results

Aligner-based long-read SV detection pipelines, as shown in pipeline A Fig. 1, rely on SV callers to resolve intra-read SVs. Commonly, long-read aligners are capable of mapping intra-read insertions and deletions by employing nonlinear models (e.g., convex model) at the cost of largely increased computational complexity. However, aligners remain less effective in mapping more complex intra-read SVs, especially nonlinear ones (e.g., inverted, duplicated and nested). The underlying cause is the alignment algorithm complexity that limits the capability of thoroughly taking into account potential rearrangements. The limitation may less impact short-read SV detection since most of them are inter-read SVs supposed to be detected by SV callers. However, due to the ultra-long lengths, long reads commonly contain a significantly larger number of intra-read SVs, which can hardly be detected by SV callers if the alignment loses the SV signals by, for

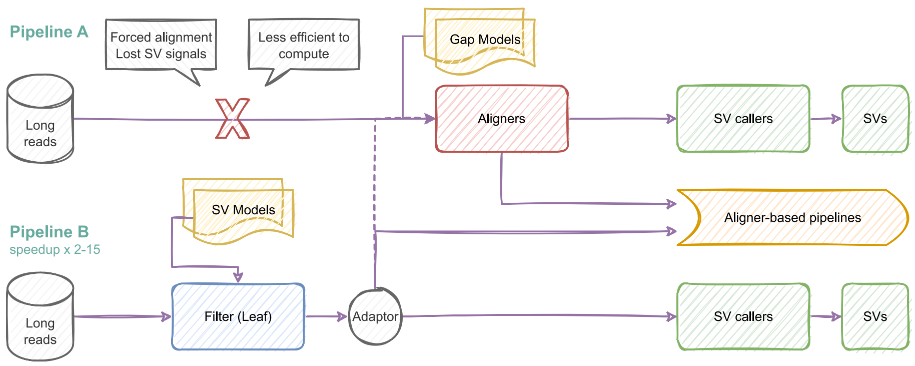

Fig. 1 The aligner-based long-red SV detection pipeline (**A**) compared to the filter-based pipeline (**B**), which applies SV models at an early stage to better capture long-read SV signals

instance, forced alignment. Therefore, a lightweight approach that can capture SV signals at an early stage would be helpful for long-read SV detection. To this end, we propose the filter-based pipeline as shown in pipeline B Fig. 1.

In the following sections, we will discuss the assessment of Leaf-based pipelines based on three high-quality datasets and benchmark tools, which include:

1. Trio-based assessments based on the Mendelian inheritance.
2. Systematical simulation of intra-read SVs for evaluating the detectable SV space.
3. Assembly-based SV calls for HiFi read insertion and deletion evaluation.

Trio-based SV call assessment

We prepared 7 datasets for the trio-based assessment:

1. Ashkenazim Jewish trio: HG002 (son), HG003 (father), and HG004 (mother) [37, 38];
2. Han Chinese trio: HG005 (son), HG006 (father), and HG007 (mother) [37]; and
3. SKBR3 breast cancer cell line [39].

We set up 4 different pipelines combining Leaf, long-read aligner minimap2 [22] with two SV callers, SVIM [40] and cuteSV [41], to call SVs in the datasets described above. First, we set the minimum number of reads to call an SV (supporting reads) 7 to get an overview of the number of SVs detected by each pipeline. Figure 2 compares the number of SVs detected by the four pipelines. Table 1 summarizes SVs $\geq$ 80 bps detected by the Leaf-cuteSV and Leaf-SVIM. We employ the relative recall [43] in the following expression to compare the number of SVs of the ith dataset detected by pipelines X and $Y \in \{A, B, C, D\}$.

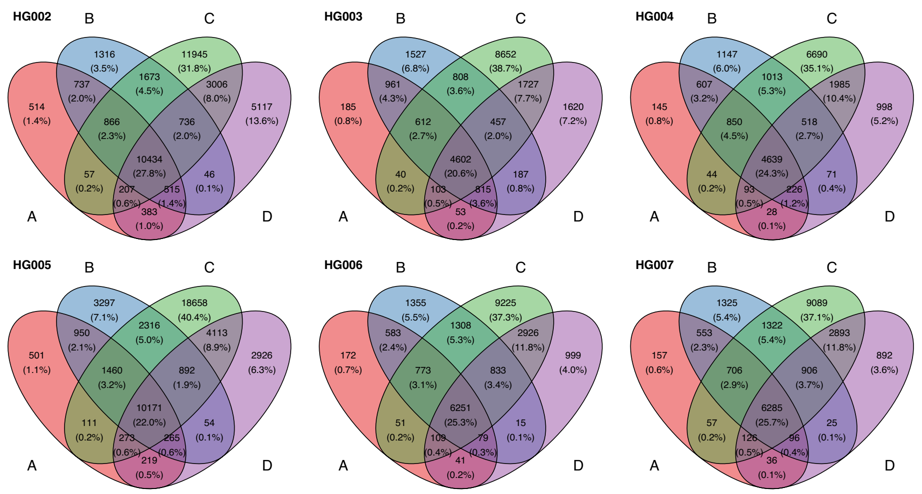

Fig. 2 Venn diagrams of SVs detected by 4 different pipelines (**A**–**D**) on 6 datasets of 2 trios, Ashkenazim Jewish trio (HG002–HG004) and Han Chinese trio (HG005–HG007). Pipeline A uses the aligner and SVIM. Pipeline B uses the aligner and cuteSV. Pipeline C uses Leaf and cuteSV. Pipeline D uses Leaf and SVIM

Table 1 Summary of SVs ($\geq$ 80 bps) detected by Leaf-SV callers ($\geq$ 80 supporting reads)

Trios	Dataset	Platform	Depth	SVs caller	Total	INS	DEL	INV	DUP
Ashkenazim	HG002 (son)	PacBio	72	cuteSV	28,924	13,261	11,819	460	3384
Jewish	HG002 (son)	PacBio	72	SVIM	20,444	9742	9943	/	759
	HG002 (son)	ONT	50	cuteSV	25,258	11,068	10,821	113	3256
	HG002 (son)	ONT	50	SVIM	17,774	7789	9985	/	/
	HG003 (father)	PacBio	32	cuteSV	17,001	7974	8006	197	824
	HG003 (father)	PacBio	32	SVIM	9564	4462	4959	/	143
	HG004 (mother)	PacBio	32	cuteSV	15,832	7155	8001	78	598
	HG004 (mother)	PacBio	32	SVIM	8558	4076	4385	/	97
Han Chinese	HG005 (son)	PacBio	63	cuteSV	37,994	21,244	13,436	431	2883
	HG005 (son)	PacBio	63	SVIM	18,913	8676	9689	/	548
	HG006 (father)	PacBio	30	cuteSV	21,476	10,215	10,193	189	879
	HG006 (father)	PacBio	30	SVIM	11,253	5414	5693	/	146
	HG007 (mother)	PacBio	30	cuteSV	21,384	10,409	9790	162	1023
	HG007 (mother)	PacBio	30	SVIM	11,259	5487	5649	/	123
/	SKBR3 cell line	PacBio	72	cuteSV	34,436	18,423	12,312	206	3495
	SKBR3 cell line	PacBio	72	SVIM	19,381	9141	9414	/	826

$$recall_{X_i|Y_i} = \frac{|X_i \cap Y_i|}{|Y_i|} = \frac{SVs\ in\ X_i\ and\ Y_i}{SVs\ in\ Y_i} \tag{1}$$

For instance, $recall_{C_2|A_2} = 0.843$ means that for HG002, pipeline C (Leaf-cuteSV) recalls 84.3% SVs detected by pipeline A (aligner-SVIM). The average relative recall over all datasets for each pipeline ($recall_{C|A} = 0.848$, $recall_{A|C} = 0.657$, $recall_{C|B} = 0.794$ and $recall_{B|C} = 0.576$) suggests that Leaf-based pipelines (C and D) recall more SVs than aligner-based pipelines (A and B).

We then employ the Mendelian inheritance [23, 41, 43] to evaluate the recall and precision of each pipeline. We preparedto evaluate the recall and precision of each pipeline. We prepared the high-confidence SV datasets denoted as T for both the Ashkenazim Jewish trios and Han Chinese trios. We established the criteria that each high-confidence SV $\in T$ must be recalled by an SV caller with a minimum of 10 supporting reads and must align with Mendelian inheritance. The comparison of two SVs involves assessing their reciprocal overlap, deeming them identical if a proportion of their individual sizes overlap, and their genotypes match. For insertions and duplications, which lack a physical span over the reference, we compare their virtual reference span defined as a span starting at the SV position and ending at the virtual endpoint an SV length away from the starting endpoint. We employed the true positive rate (TPR), Mendelian discordance rate (MDR), and recall of homozygous (RH) given by the following expressions for evaluation,

$$TPR = recall_{son|T} = \frac{son's\ true\ SVs}{true\ SVs}$$

$$MDR = recall_{\overline{parents}|son} = \frac{son's\ SVs\ not\ detected\ in\ parents}{son's\ SVs}$$

$$RH = recall_{son|parents\ homozygous} = \frac{parents\ homozygous\ SVs\ detected\ in\ son}{parents\ homozygous\ SVs}$$

where $recall_{X|Y}$ is the relative recall defined in expression Eq. 1.

Table 2 summarizes TPRs, MDRs, and RHs of the four pipelines applied to the two trios. The results suggest aligner-based pipelines have relatively better MDRs and RHs, while Leaf-based pipelines have much better TPRs. MDRs ($> 10\%$) of both types of pipelines are significant, particularly when combined with cuteSV, revealing that some SVs detected in sons do not follow Mendelian inheritance. However, they are largely attributable to the lower read coverage of parents ($30\times$) compared to sons ($72\times$). Moreover, it is also worth noting that the two SV callers perform differently in terms of recall and precision. SVIM generates fewer false positives (lower MDRs and higher RHs), while cuteSV reports more true SVs (higher TPRs). The statistics suggest SVs recalled by the four pipelines are basically in line with the Mendelian inheritance, while Leaf-SV callers reported more SVs that passed the Mendelian inheritance validation.

Read coverage is critical to population-scale long-read SV analysis due to the sequencing cost. Hence we assessed the precision, recall, and F_1 score (F-measure) as shown in the following expression corresponding to the number of supporting reads for calling SVs.

$$F_1 = 2 \cdot \frac{recall \cdot precision}{recall + precision}$$

The results are shown in Fig. 3, where the axis of coverage is the minimum supporting reads to recall an SV. It shows SVIM-based pipelines are of similar performances, while the cuteSV-based pipelines exhibit notable differences. Leaf-cuteSV has the highest recall at all levels of coverage. Its precision is lower than aligner-cuteSV, especially when coverage < 7, while the precision increases quickly and becomes comparable when coverage ≥ 8. Leaf-cuteSV with 8 to 10 supporting reads achieves the most balanced performance (i.e., highest F_1 score).

Nested SVs are known to be associated with diseases, while SVs nested in long reads are commonly more difficult for aligner-based pipelines to resolve. We analyzed nested SVs comprising two basic SVs (i.e., INS, DEL, INV, DUP), such as inverted duplication (INVDUP), insertion nested inversion (INVINS), deletion nested inversion (INVDEL), and deletion nested duplication (DUPDEL), based on the results of

Table 2 True positive rate (TPR), Mendelian discordance rate (MDR) and recall of homozygous (RH) for the two trios. Highlighted numbers are better

Trios	SVs caller	TPR[%]		MDR[%]		RH[%]	
		Leaf	Aligner	Leaf	Aligner	Leaf	Aligner
Ashkenazim Jewish	cuteSV	**93.21**	67.98	24.40	**22.16**	89.13	**95.46**
	SVIM	**63.10**	57.04	18.70	**8.88**	**99.02**	98.07
Han Chinese	cuteSV	**88.88**	70.04	**18.90**	21.90	93.61	**96.23**
	SVIM	55.61	**56.67**	9.67	**6.79**	97.57	**97.70**

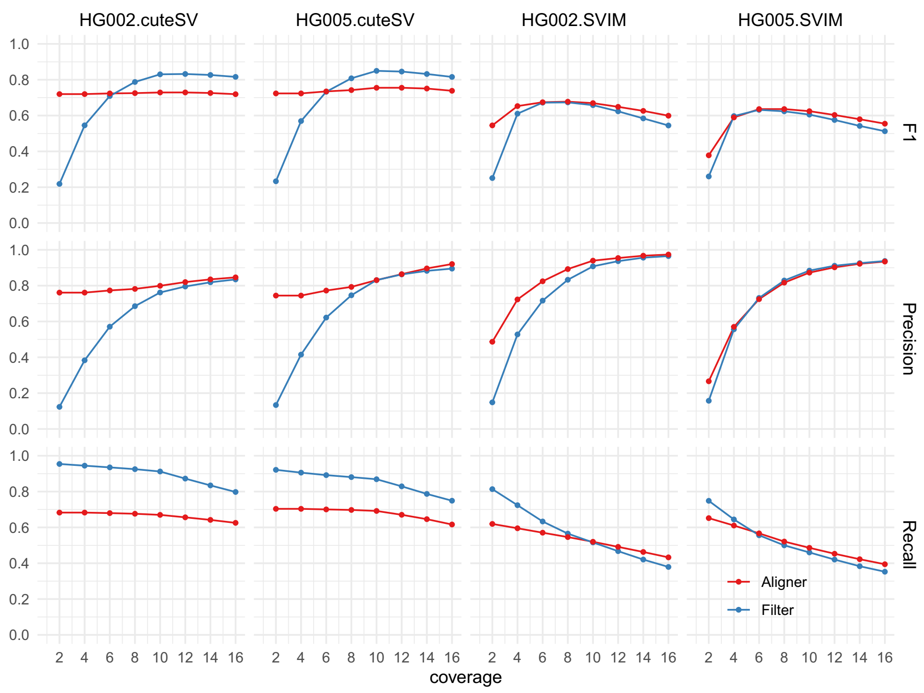

Fig. 3 F_1 score, precision and recall for 4 pipelines across datasets of two sons (i.e., HG002 and HG005). The horizontal axis of coverage is the minimum number of supporting reads to recall an SV

Table 3 Comparison of nested SVs found in the results of Leaf- and aligner(Aln)-cuteSV

Dataset	Total		INVDUP		INVINS		INVDEL		DUPDEL	
	Leaf	Aln	Leaf	Aln	Leaf	Aln	Leaf	Aln	Leaf	Aln
Ashkenazim Jewish son	127	66	17	3	7	4	7	9	96	50
Ashkenazim Jewish parents	91	29	18	1	4	3	3	3	66	22
Han Chinese son	189	85	21	3	9	10	9	14	150	58
Han Chinese parents	85	51	14	3	5	1	5	5	61	42
SKBR3	58	56	9	3	8	3	3	8	38	42

Leaf- or aligner-SV caller pipelines. Table 3 summarizes the number of nested SVs found in the trio-based datasets and SKBR3 dataset. We did not assess the recall and precision due to lacking nested SV callers [18, 44]. Figure 4 shows two highly nested SVs comprising four basic ones in SKBR3 found by Leaf-cuteSV. It is to show the potential of filter-based pipelines in detecting highly nested SVs.

Detectable SV space assessment

In this assessment, we systematically simulated intra-read SVs for measuring the detectable SV space of Leaf- and aligner-based pipelines. The long-read SV space in the assessment comprises three key attributes: SV type, SV length and sequencing error. We used long-read simulators PBSIM and NanoSim [45] to simulate PacBio and ONT reads sequenced from GRCH38 with the average sequencing errors of 10%, 15%, and 20%. SV types including insertion, deletion, duplication, and inversion of lengths ranging

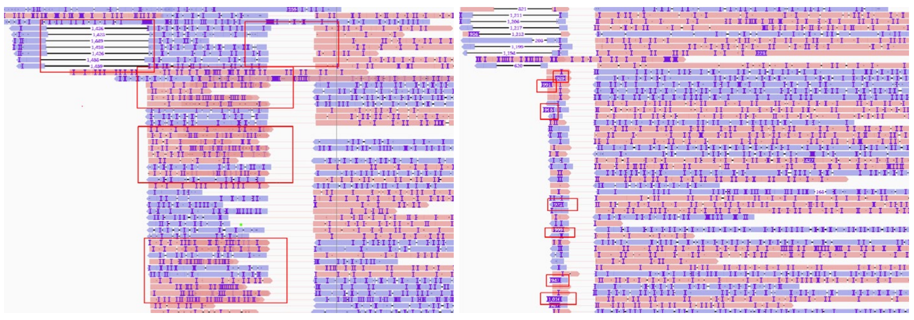

(a) Two DELs, one DUP, and one INV (b) Two DELs, one INS, and one INV

Fig. 4 Highly nested SVs found in the SKBR3 breast cancer cell line by Leaf-cuteSV. Images are generated by Integrative Genomics Viewer (IGV). Sequences of different strands are highlighted with different colors. The nested SV in the first subfigure comprises two deletions of 1441 bps and 750 bps on the two sides and one 976-bps duplication in darker red embedded in the inversion. The nested SV in the second subfigure comprises two deletions and one 987-bps insertion highlighted by rectangles embedded in the inversion

from 100 bps to 2×10^3 bps are simulated and planted into simulated reads at random positions. We also employed two advanced long-read aligners, minimap2 and NGMLR [23] as the control. Then we ran Leaf and aligners and evaluated recall and precision by directly comparing the planted SV endpoint deviation, which is the distance between the detected SV endpoints and the planted ones, without using an SV caller since the planted SV endpoints are known. An SV is regarded as correctly identified if all endpoint deviations ≤ 50 bps.

Figure 5 shows the detectable SV space measured by recall and precision. As expected, aligners performed better in detecting insertions and deletions mostly because of the nonlinear gap model (e.g., convex gap model), which can distinguish between short indels of sequencing errors and longer insertions or deletions of SVs. However, the aligners are ineffective in mapping nonlinear intra-read SVs such as inversions and duplications as shown in the second and third rows of the figure. By contrast, Leaf is comparable to the aligners in detecting insertions and deletions, while it remains effective in mapping nonlinear SVs, such as inversions of 200 bps to 500 bps missed by aligners. Overall, Leaf shows more complete detectable SV space than aligners. The assessment suggests that canonical long-read pipelines, such as aligner-SV callers, could be substantially less effective in detecting nonlinear intra-read SVs. It is largely attributable to the incomplete space of aligners, which may lose critical SV signals, while the filter-based pipelines, which capture SV signals at an early stage, such as Leaf in the assessment, have the potential to complement the detectable SV space and thus enhance the capability of canonical pipelines in detecting complex SVs.

Assembly-based SV call assessment

In this assessment, we evaluated the performance of Leaf-SV caller pipelines based on assembly-based insertion and deletion calls. The assessment workflow is shown in Additional File 1: Fig. S1. Specifically, we prepared an insertion and deletion dataset by applying pipeline dipcall [46] to the Human Pangenome Reference Consortium (HPRC) diploid assembly of HG00733 as the true SV set for evaluation. We then used the public

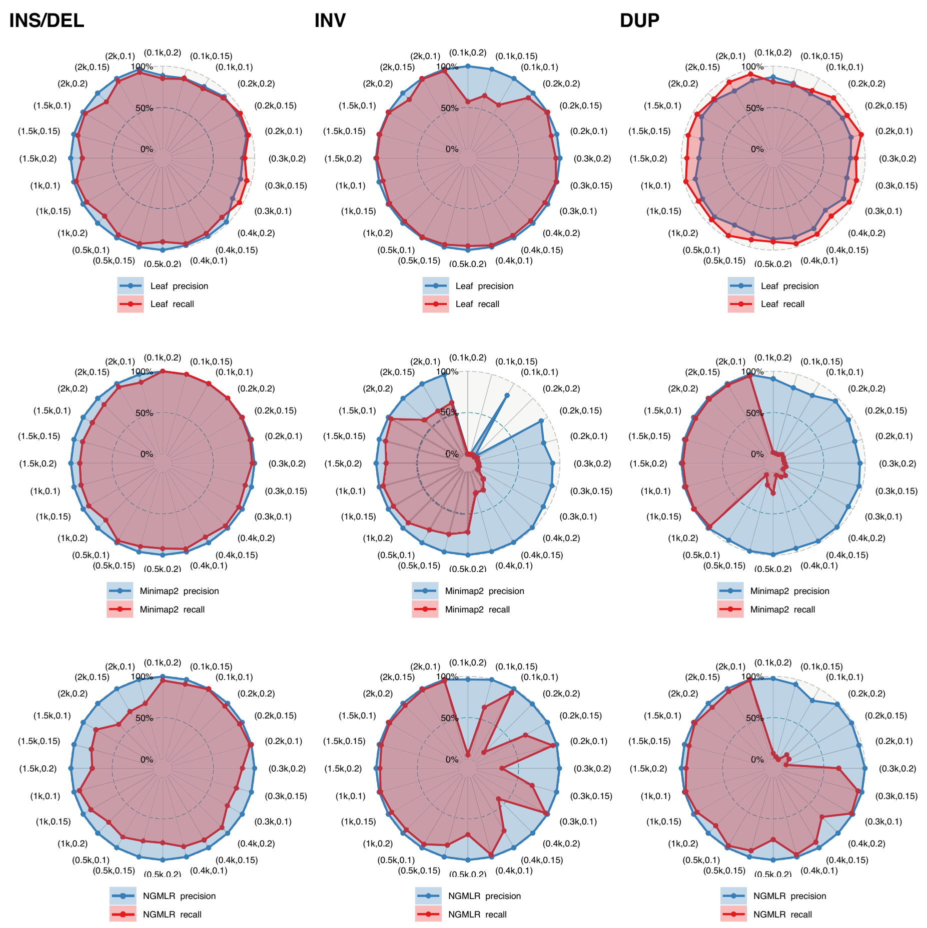

Fig. 5 Detectable SV space of Leaf and aligners measured by the recall and precision of detecting systematically simulated SVs. Values in the figure are labeled by tuples of SV length (bps) and the sequencing error

dataset of HG00733 PacBio HiFi reads as the read datasets and applied Leaf, minimap2, and NGMLR with cuteSV and SVIM to the reads for SV calling. Finally, we compared SVs detected by the four pipelines to the assembly-based SV set by using the benchmark toolkit Truvari [43]. It is worth noting that the datasets of assessment are prepared based on minimap2. Specifically, dipcall is a pipeline employing minimap2 for aligning genome to HPRC assembly, which is also assembled by hifiasm developed by the team of minimap2. Additionally, both the HPRC assembly and the read dataset for testing are HG00733 PacBio HiFi reads. In such a case, the assessment essentially employs minimap2 as the benchmark for evaluating the precision and recall of other pipelines. Hence minimap2 in this test is employed as the reference bounds of recall and precision, and another different NGMLR-based pipeline is employed as the bias (confounder) control.

Figure 6 shows the assessment results, where recall of Leaf is higher than that of NGMLR and is close to minimap2 in the assessment. Due to the assessment bias discussed above, the relative $recall_{Leaf|minimap2}$ defined in expression Eq. 1, is a better metric for recall assessment. Additional File 1: Table S1 summarizes the relative recall of Leaf-based pipelines. It suggests Leaf-SV callers can recall most insertions and deletions detected by minimap2-SV callers. On the other hand, the relatively lower precision of

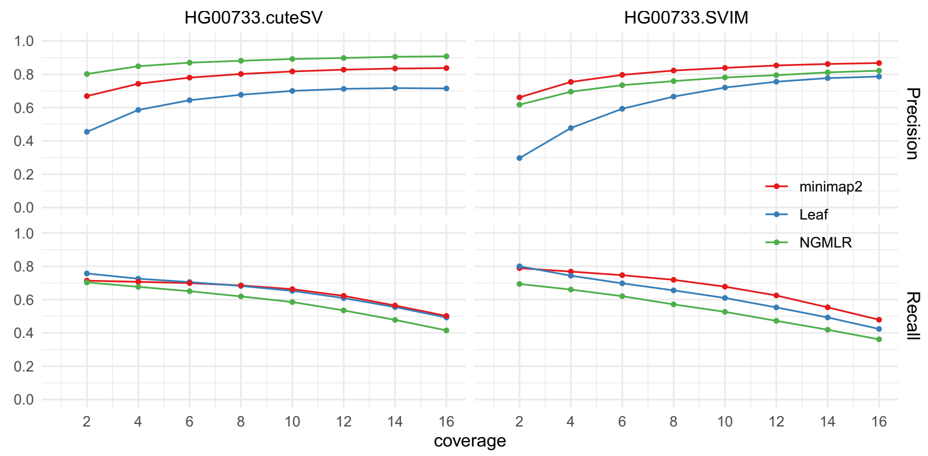

Fig. 6 Results of detecting insertions and deletions in HG00733 for the six pipelines. The precision and recall are evaluated by comparing the results to the true SV set generated by minimap2-based pipelines (dipcall). The axis coverage is the minimum number of supporting reads to call an SV

Leaf-based pipelines is attributable to that Leaf reported more SVs. However, it conforms to the general design principle of filters, where sensitivity commonly takes priority over others including precision, which can be easily improved in the validation stage. Moreover, a number of false positives are potential true SVs missed by dipcall. Existing research suggests this number could be upper to 15% [47]. Thus the real recall and precision of Leaf could be substantially higher.

Computational performance assessment

Finally, we assessed the computational performance of Leaf- and aligner-based (i.e., minimap2 and NGMLR) pipelines. Without loss of generality, we used PacBio raw reads of the HG002 dataset for the evaluation instead of HiFi reads since it is commonly more computationally intensive to process raw reads. We evaluated the runtime and memory footprint for running Leaf, minimap2 and NGMLR. Both aligners apply the single instruction multiple data (SIMD), which is a parallelism technique for hardware acceleration, to accelerate the gap model for insertion and deletion detection. Therefore, they run much faster than many other long-read aligners. We evaluated the elapsed time as well as the CPU time, which is a better metric for assessing algorithm complexity excluding I/O. In the results as shown in Fig. 7, Leaf runs significantly faster than the aligners. It is worth noting that the runtime in the figure is in $\log_{10}$ scaled. The elapsed time scales nonlinearly for a growing number of threads are attributable to the limitation of Amdahl's law. Particularly, reading and writing large sequenced files gradually becomes the computational bottleneck as threads increase.

Moreover, we assessed the runtime of long-read SV callers (SVIM, cuteSV, and PBSV) when they took the results of Leaf and the aligners as input. We used the default parameters of each SV caller for the assessment. We expected Leaf-SV callers to run faster because Leaf outputs more concise SAM/BAM than aligners for PacBio raw reads. In the results shown in Fig. 7, SVIM is single-threaded and runs approximately 1.75× faster when taking as input the results of Leaf. cuteSV takes as input the results of Leaf runs

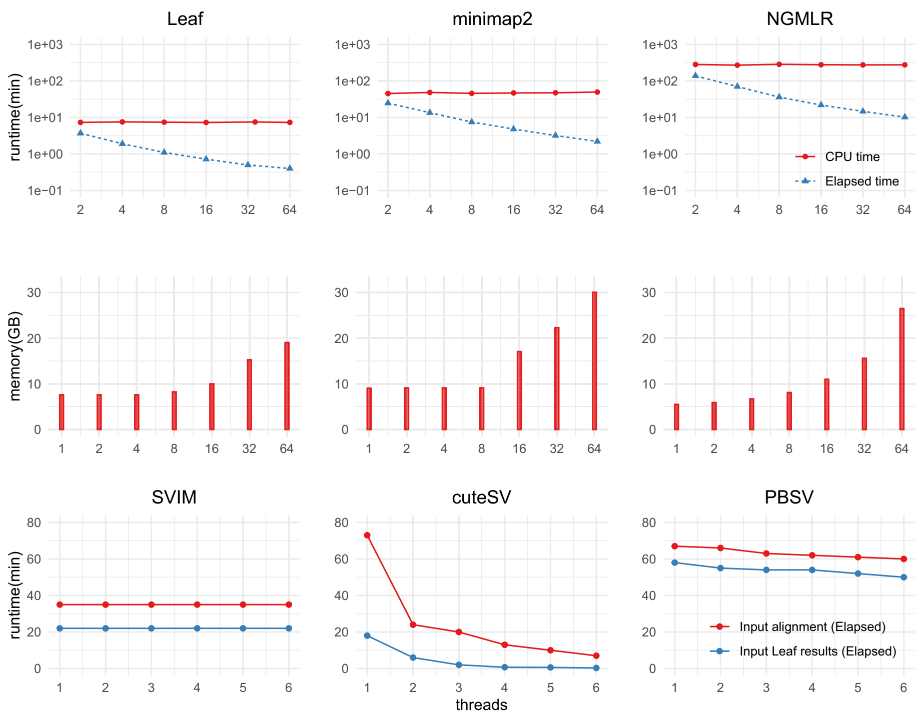

Fig. 7 Runtime and memory footprint assessment: The first and second rows are the time and maximum resident memory of Leaf and aligners. CPU time is the amount of time for which the CPU is used. Elapsed time is the time for which the program runs. Vertical axes in the first row are in $\log_{10}$ scaled. The last row is the runtime of SV callers taking alignment and Leaf results of PacBio CLR reads as input

over 3× faster. PBSV combined with Leaf runs approximately 1.2× faster using either a single thread or multiple threads. The assessment suggests that filter-based pipelines, such as Leaf-based ones, could be more computationally efficient than conventional pipelines.

Discussion

We conducted different kinds of assessments in this work to reduce the potential biases caused by the complexity and diversity of long-read SVs. Despite the assessment differences, the results are essentially in accordance with the expectation that Leaf-SV callers can achieve comparable precision while outperforming aligner-SV callers in computational efficiency and sensitivity, particularly for nonlinear intra-read SVs. For instance, the assembly-based assessment for detecting insertions and deletions in HiFi reads is in line with the trio-based assessment. Both the assessments suggest $recall_{Leaf|Aligner} \approx 1$ defined in expression Eq. 1. Namely, most true insertions and deletions detected by aligners can also be detected by Leaf. Additionally, the assembly-based assessment of HiFi read is also in line with the detectable SV space assessment (i.e., sequencing error 0.1 in column INS/DEL Fig. 5). Moreover, both the trio-based assessment and SV space assessment suggest Leaf performs better in detecting nonlinear intra-read SVs such as intra-read inversions. It is in line with the expectation that capturing SV signals at an early stage can enhance the performance of SV detection pipelines.

As a new type of pipeline, limitations exist that could be addressed in the future. Although the outputs of Leaf are compatible with SV callers, the performance of Leaf-SV caller pipelines can be further improved. For instance, endpoints of SV signals reported by Leaf are commonly more divergent than aligners, as shown in Additional File 1: Fig. S2. In consequence, existing alignment-based SV callers are more likely to fail in computing the consensus endpoints of supporting reads. We found in the assessment that a considerable number of SV signals were detected by Leaf but could not be recalled by SV callers due to endpoint divergence. Therefore the performance of Leaf-SV caller pipelines can be further improved by improving the consensus of endpoint. To this end, we can align a short sequence containing endpoints of the SV signals to reduce the endpoint divergence. It is simple to implement and is compatible with existing alignment-based SV callers. Another solution is to develop a brand new filter-based SV caller. Although it would be more complex to implement, the performance of filter-based pipelines would potentially be fully exploited.

Conclusion

In this work, we proposed a new filter-based pipeline for population-scale long-read SV detection. The core idea of the filter-based pipeline is to capture SV signals at an early stage, which are likely missed by many long-read aligners. To this end, we implemented Leaf and conducted comprehensive assessments in this work, which suggest Leaf has the following features and benefits compared to aligners: First, it is comparable to aligners in terms of mapping insertion and deletion detection. Second, it has an outstanding performance in mapping nonlinear intra-read SVs. Third, it is much more computationally efficient than long-read aligners. Finally, Leaf is a technical validation revealing the feasibility and potential of long-read filter-based pipelines. The performance of the filter-based pipelines can be further improved as a growing number of optimizations are employed.

Methods

Here, we discuss the main methods employed by Leaf, which consists of four modules:

1. A canonical binning module for quick clustering patterns in long reads. It takes long reads as input and output clustered anchors of matched patterns in the read and the reference.
2. An adversarial autoencoder (AAE) for screening discordant anchors and computing priors of potential SV gaps.
3. A generative module for computing the likelihoods of each potential assembly of anchors and generating the most likely SV mappings.
4. An adaptation module for trimming and adapting the results to the format compatible with SV callers.

Anchor binning

In the first module, the canonical binning is employed to cluster anchors. We use the refined minimizers [48] as the patterns for binning, which can be briefly described as follows. Denote $p_{ij} = (h_{ij}, x_{ij})$ as the *j*th pattern sampled from the sequence *i*, where h_{ij} is the hash value of the pattern and x_{ij} is the position of p_{ij}. Given two matched patterns (p_{gi}, p_{rj}) from genome *g* and read *r*, whose hash values are identical (i.e. $h_{gi} = h_{rj}$), denote $A_{ij} = x_{gi} - x_{rj}$ as the anchor of p_{gi} and p_{rj}. A_{ij} within the given bound are clustered into bins. Specifically, the key to the bin for anchor A_{ij} is given by $key = \lfloor A_{ij}/n \rfloor$, where constant n is the interval of the bin, and $\lfloor \cdot \rfloor$ is the floor operator. We built a genome index to speed up the binning process, where anchors are collected by streaming read *r* and querying the index for matched patterns. Bins containing sufficient anchors are then selected for likelihood computation in the next stage.

AAE for priors

Due to sequencing errors and intra-read SVs of long reads, discordant anchors exist that constitute gaps. We conduct a preliminary screening of discordant anchors at this stage to classify and assign SV priors. The screening results are used to help initiate the generative model in the next stage. Intuitively, the idea of the screening is to generate an overall impression of whether the anchors are likely from SVs and then initiate the generative model by passing a continuous variable, the prior. Without the screening, we may discretely classify a gap > 50 bps for instance, as a potential indel signal (i.e., prior $= 0$ or 1), while the screening may assign indel prior, probably 0.6, to a gap of 50 bps. It helps better process intra-read SV signals. The prior function for discordant anchors involves latent relations regarding gap shape and size, etc., which may be hard to define explicitly. A workable solution is to employ a trained network. We implemented an adversarial autoencoder (AAE) prototype to help initialize SV priors for discordant anchors. The AAE implementation is further described in Additional File 1: Section 3.1. It is worth noting that the screening does not generate the final results (i.e., sequence mappings). Instead, it is used to aid the generative model, which generates accurate mappings and is independent of the training data.

Generative model

We use the generative model to generate the most likely assembly of fragments from which the given read is sequenced. The core idea is to use likelihood [49] functions instead of score functions to compute the optimal assembly of fragments. Intuitively, it is more reasonable to use smooth likelihood functions involving multiple variables for modeling the assembly of fragments.

Denote a_i as the subassembly from which the subread $r_i, i = 1, 2, ..$ is sequenced. Assuming a_i and r_i depend on parameters $\Theta = \{\theta_1, \theta_2..\}$, (e.g., sequencing error *e*, length *l*, and SV *v*) then the likelihood that r_i is sequenced from a_i is given by

$$\mathcal{L}(a_i; r_i) = p(r_i|a_i) \approx p(\Theta)$$

Assuming *e*, *l*, and *v* are the main parameters in Θ and the fragment (a_i, r_i) comprises a subfragment of map $(a_{m,i}, r_{m,i})$ and an independent subfragment of SV gap $(a_{g,i}, r_{g,i})$ at the $5'$ end, then the likelihood above is approximated by

$$\begin{aligned} p(r_i|a_i) &= p(r_{m,i}|a_{m,i})p(r_{g,i}|a_{g,i}) \approx p_m(\Theta)p_g(\Theta) \\ &\approx p_m(e_{m,i}, l_{m,i})p_g(e_{g,i}, l_{g,i}, v_{g,i}) \end{aligned}$$

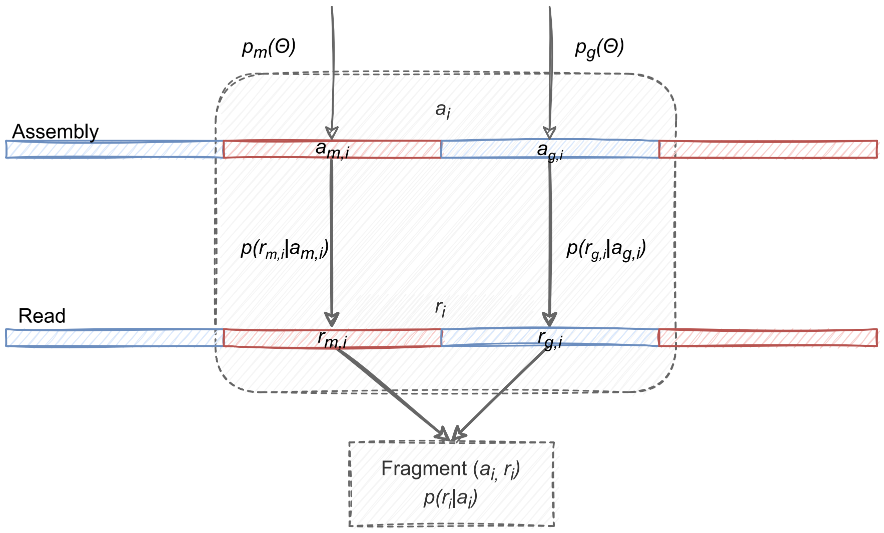

Fig. 8 Fragment likelihood $p(r_i|a_i)$ model, which is the probability that subread r_i is sequenced from subassembly a_i. The *i*th fragment (a_i, r_i) is dived into independent map $(a_{m,i}, r_{m,i})$ (red) and gap $(a_{g,i}, r_{g,i})$ (blue). $p(r_i|a_i)$ correspondingly comprises $p(r_{m,i}|a_{m,i})$ and $p(r_{g,i}|a_{g,i})$. The two likelihoods are approximated by p_m and p_g, which are functions of observable variables Θ

where p_m and p_g are the map and gap probabilities as shown in Fig. 8. Provided sequencing error e is constant for a given read, we use $p_{g,e}(l, v)$ to denote $p_g(e, l, v)$ in the following discussion. Assume v comprises n independent basic SVs (or gap) $v_j \in$ {indel, inversion, duplication, reg...} nested in the gap, where "reg" refers to the regular gap free of any SV. Formally, denote $v = \bigcup_{j=1}^{n} v_j$ the nested SV in g then $p_{g,e}(l, v)$ is given by

$$p_{g,e}(l,v) = p_{g,e}\left(l, \bigcup_{j=1}^{n} v_j\right) = \sum_{j=1}^{n} p_{g,e}(l, v_j) - \sum_{j=1}^{n}\sum_{k=1}^{j} p_{g,e}(l, v_j)p_{g,e}(l, v_k) + ... \quad (2)$$

We use expression Eq. 2 to integrate an arbitrary number of SVs (v_j) into the gap model, while restrictions on coexistence of v_j are further defined in Additional File 1: Table S2. Expression Eq. 1 applies to probabilities of nested SVs as well as single basic ones. For instance, the probability of a basic indel gap can be expressed by simply setting probabilities of reg, inversion and duplication 0 or a small value in expression Eq. 2.

Then we define $p_{g,e}(l, v_j)$ in expression Eq. 2. Assume the gap of l in length comprises the gap in the assembly of l_x in length and the gap in the read of l_y in length, then $p_{g,e}(l, v_j)$ is given by

$$p_{g,e}(l, v_j) = p_{g,e}(v_j)p_{g,e}(l|v_j) = \omega_{v_j} p_{g,e}(l|v_j) = \omega_{v_j} p_{g,e}(l_x, l_y|v_j) \quad (3)$$

where $\omega_{v_j} = p_{g,e}(v_j)$ is the prior of v_j. $p_{g,e}(l_x, l_y|v_j)$ regarding each v_j are defined in Additional File 1: Section 3.2. Plugging $p_{g,e}(l_x, l_y|v_j)$ into expression Eq. 2, we have $p_{g,e}(l_x, l_y, v)$ visualized in Fig. 9, where free variables ω_v and ω_r are priors of SVs and regular gap. For instance, for a gap of $l_x = 150$ and $l_y = 0$, which is likely a deletion of 150*bps* in length, $p_{g,e}$ in subfigure (a) of smaller ω_v outputs a lower likelihood at point (150, 0), while $p_{g,e}(l_x, l_y, v)$ in subfigure (c) of larger ω_v outputs a higher likelihood at point (150, 0).

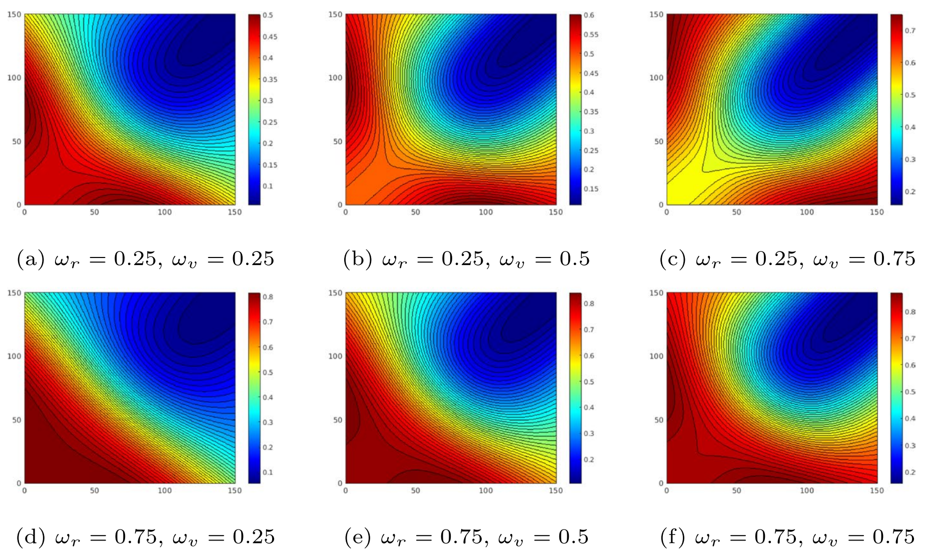

(a) $\omega_r = 0.25,\ \omega_v = 0.25$ (b) $\omega_r = 0.25,\ \omega_v = 0.5$ (c) $\omega_r = 0.25,\ \omega_v = 0.75$

(d) $\omega_r = 0.75,\ \omega_v = 0.25$ (e) $\omega_r = 0.75,\ \omega_v = 0.5$ (f) $\omega_r = 0.75,\ \omega_v = 0.75$

Fig. 9 Contour lines of likelihood $p_{g,e}(l_x, l_y, v) \in [0, 1]$ defined in expressions Eqs. 2 and 3. Horizontal (l_x) and vertical (l_y) axes in each subfigure are gap lengths of the assembly and read. w_r and w_v are the priors of regular gaps and SV (indel) gaps

Moreover, each subfigure has the lowest probability at point (150, 150), which is likely to be an incorrect gap rather than a regular gap or SV gap. It is worth noting that models for $p_{g,e}(l|v_j)$ are not limited to the ones in the Additional File 1: Section 3.2. For instance, variables $\theta_i \in \Theta$ other than l possibly better fit the SV probabilities (i.e. $p_{g,e}(\Theta|v_j)$).

Finally, we compute the most likely assembly denoted by $\hat{A}_i$ for $r_1, .., r_i$. Assuming each r_i is sequenced independently from the assembly, the likelihood of at least one subsequence $r_1, r_2, ..., r_i$ being sequenced from A_i is given by

$$\mathcal{L}_i = \mathcal{L}(A_i; r_1, r_2, ..., r_i) = (1 - p(r_i|a_i)) \cdot \mathcal{L}_{i-1} + p(r_i|a_i) \tag{4}$$

$\mathcal{L}_i$ is computed by dynamic programming (DP) and $\hat{A}_i$ is the one that maximizes $\mathcal{L}_i$.

Adaptation

Extended SAM/BAM

The standard SAM/BAM is a widely used alignment format. We adapt the results of the generative model to SAM/BAM by extending the meaning of the columns in the standard SAM/BAM format. The standard SAM/BAM records base-to-base alignment, which is a pair of two identical bases whose positions in the sequences can be denoted by a tuple of (x, y). However, the concept of identical bases does not apply to the results of the generative model, whose bases involve the concept of likelihood. To this end, we extended the meaning of SAM/BAM by introducing the concept of deviation d to the tuple, namely $(x, y) \to (x, \hat{y}, d)$, where $d = y - \hat{y}$ is the deviation between base y and its estimation denoted by $\hat{y}$. Since d is commonly randomly varied, we denote D as the random variable over all possible d and use tuple $(x, \hat{y}, D)$ to express the results of the generative model. To record tuple $(x, \hat{y}, D)$, we employ the cigar string of the standard SAM/BAM to record $(x, \hat{y})$, while it is not necessary to explicitly record D for each cigar since it commonly follows a distribution determined by the model. For instance, in the case of the generative model, if D follows a normal distribution suggesting x is likely to be sequenced from one of the bases around $\hat{y}$ then we can record the mean μ and variance σ^2 in the headers or operational fields of SAM/BAM. Therefore, existing fields in the standard SAM/BAM are sufficient for recording the tuple $(x, \hat{y}, D)$. Exact definitions for each field in the extended SAM/BAM are discussed in Additional File 1: Section 3.3. Finally, it is worth noting that standard SAM/BAM of alignment is a special case of extended SAM/BAM discussed above, where x is regarded as always sequenced from $\hat{y}$ (i.e., $D \equiv 0$). Therefore, the definition above is an extension of the standard SAM/BAM and it applies to alignments as well.

Software compatibility

We tested the compatibility of the extended SAM/BAM for the following toolkits. In principle, they can be directly combined with Leaf without adjustment. However, the interpretation of the toolkit output should be changed correspondingly when taking extended SAM/BAM as input. Especially, the deviation concept should always be taken into account when applying the extended SAM/BAM to them.

1. SAMtools version 1.10: It is the toolkit for SAM/BAM operations. Three SAMtools modules used in this work were tested. They are SAMtools view, SAMtools index, and SAMtools sort for viewing and indexing SAM/BAM.
2. IGV version 2.8.3: It is the sequence visualization tool. The results of Leaf can be visualized directly by IGV. It is also worth noting that gaps shorter than the deviation, commonly < 50 bps, in the visualized results should be ignored since they are insignificant.
3. PBSV version 2.3.0: PBSV is an SV caller for PacBio sequencing reads. It takes SAM/BAM files as input. The sample name and read group should be specified in the SAM header when using PBSV. The compatibility of Leaf with PBSV was tested. The results can be processed directly by PBSV with default settings.
4. SVIM version 1.2.0: SVIM is an SV caller for PacBio and ONT reads. It takes the SAM/BAM as input. The compatibility of Leaf with SVIM was tested. Leaf results can be processed directly by SVIM. It is better to use the default arguments for either PacBio CLR or HiFi reads when combined with Leaf due to the deviations discussed above.
5. cuteSV version 1.0.13: cuteSV is an SV caller for PacBio and ONT reads. It takes as input the SAM/BAM as well. The compatibility of Leaf with cuteSV was tested. Leaf results can be processed directly by cuteSV. We also suggest to use default arguments for different types of long reads.

Supplementary Information

The online version contains supplementary material available at https://doi.org/10.1186/s13059-024-03297-5.

Additional file 1. Supplementary figures, tables and methods.

Additional file 2. Peer review history.

Acknowledgements
We thank the Sequence Analysis library (SeqAn) project and the German Network for Bioinformatics Infrastructure (de.NBI) for computational infrastructure support.

Review history
The review history is available as Additional file 2.

Peer review information
Tim Sands was the primary editor of this article and managed its editorial process and peer review in collaboration with the rest of the editorial team.

Authors' contributions
Knut Reinert conceived and outlined the project. Chenxu Pan developed the model and conducted the assessment. All authors read and approved the manuscript.

Funding
Open Access funding enabled and organized by Projekt DEAL. This work was supported by the Intel Parallel Computing Center (IPCC) program at FU Berlin and the Chinese Scholarship Council (CSC).

Availability of data and materials
Leaf source code is available at https://github.com/xp3i4/linear under the BSD license. An archived version is available on Zenodo [50]. Datasets used in the trio-based assessment include: Ashkenazim Jewish trio [37, 38], Han Chinese trio [37], whose sequencing data is available at GIAB ftp site ftp://ftp-trace.ncbi.nlm.nih.gov/giab or NCBI SRA linked to PRJNA200694. SKBR3 breast cancer cell line dataset is available in study [39], whose sequencing data is available on NCBI BioProject linked to PRJNA476239. Datasets for SV space assessment are available on Zenodo [51]. Datasets used in the assembly-based assessment include HPRC diploid assembly of HG00733, which is available in study [52] (https://github.com/human-pangenomics). HG00733 PacBio HiFi reads is a dataset in study [53], whose sequencing data is available at site https://s3-us-west-2.amazonaws.com/human-pangenomics/index.html or NCBI SRA with accession number ERX3831682.

Declarations

Ethics approval and consent to participate
Not applicable.

Consent for publication
Not applicable.

Competing interests
The authors declare that they have no competing interests.

Received: 28 November 2022 Accepted: 4 June 2024
Published online: 13 June 2024

References
1. De Coster W, et al. Towards population-scale long-read sequencing. Nat Rev Genet. 2021;22(9):572–87. https://doi.org/10.1038/s41576-021-00367-3. Nature Publishing Group.
2. Wenger AM, et al. Accurate circular consensus long-read sequencing improves variant detection and assembly of a human genome. Nat Biotechnol. 2019;37(10):1155–62. https://doi.org/10.1038/s41587-019-0217-9. https://www.nature.com/articles/s41587-019-0217-9. Nature Publishing Group.
3. Payne A, et al. BulkVis: a graphical viewer for Oxford nanopore bulk FAST5 files. Bioinformatics. 2019;35(13):2193–8. https://doi.org/10.1093/bioinformatics/bty841.
4. Valle-Inclan JE, et al. Optimizing Nanopore sequencing-based detection of structural variants enables individualized circulating tumor DNA-based disease monitoring in cancer patients. Genome Med. 2021;13(1):86. https://doi.org/10.1186/s13073-021-00899-7.
5. Amarasinghe SL, et al. Opportunities and challenges in long-read sequencing data analysis. Genome Biol. 2020;21(1):30. https://doi.org/10.1186/s13059-020-1935-5.
6. Mitsuhashi S, et al. Long-read sequencing for rare human genetic diseases. J Hum Genet. 2020;65(1):11–9. https://doi.org/10.1038/s10038-019-0671-8. Nature Publishing Group.
7. Sakamoto Y, et al. A new era of long-read sequencing for cancer genomics. J Hum Genet. 2020;65(1):3–10. https://doi.org/10.1038/s10038-019-0658-5. https://www.nature.com/articles/s10038-019-0658-5. Nature Publishing Group.
8. Tian L, et al. Long-read sequencing unveils IGH-DUX4 translocation into the silenced IGH allele in B-cell acute lymphoblastic leukemia. Nat Commun. 2019;10(1):2789. https://doi.org/10.1038/s41467-019-10637-8.
9. Vollger MR, et al. Long-read sequence and assembly of segmental duplications. Nat Methods. 2019;16(1):88–94. https://doi.org/10.1038/s41592-018-0236-3. https://www.nature.com/articles/s41592-018-0236-3
10. Sanchis-Juan A, et al. Complex structural variants in Mendelian disorders: identification and breakpoint resolution using short- and long-read genome sequencing. Genome Med. 2018;10(1):95. https://doi.org/10.1186/s13073-018-0606-6.

11. Beyter D, et al. Long-read sequencing of 3,622 Icelanders provides insight into the role of structural variants in human diseases and other traits. Nat Genet. 2021;53(6):779–86. https://doi.org/10.1038/s41588-021-00865-4. https://www.nature.com/articles/s41588-021-00865-4. Nature Publishing Group.
12. Wang T, et al. The Human Pangenome Project: a global resource to map genomic diversity. Nature. 2022;604(7906):437–46. https://doi.org/10.1038/s41586-022-04601-8. https://www.nature.com/articles/s41586-022-04601-8. Nature Publishing Group.
13. Kou Y, et al. Evolutionary Genomics of Structural Variation in Asian Rice (Oryza sativa) Domestication. Mol Biol Evol. 2020;37(12):3507–24. https://doi.org/10.1093/molbev/msaa185.
14. Alonge M, et al. Major impacts of widespread structural variation on gene expression and crop improvement in tomato. Cell. 2020;182(1):145-161.e23. https://doi.org/10.1016/j.cell.2020.05.021.
15. Liu Y, et al. Pan-Genome of Wild and Cultivated Soybeans. Cell. 2020;182(1):162-176.e13. https://doi.org/10.1016/j.cell.2020.05.023.
16. Chander V, et al. Evaluation of computational genotyping of structural variation for clinical diagnoses. GigaScience. 2019;8(9):giz110. https://doi.org/10.1093/gigascience/giz110.
17. Johnson JS, et al. Evaluation of 16S rRNA gene sequencing for species and strain-level microbiome analysis. Nat Commun. 2019;10(1):5029. https://doi.org/10.1038/s41467-019-13036-1.
18. Mahmoud M, et al. Structural variant calling: the long and the short of it. Genome Biol. 2019;20(1):246. https://doi.org/10.1186/s13059-019-1828-7.
19. Sedlazeck FJ, et al. Piercing the dark matter: bioinformatics of long-range sequencing and mapping. Nat Rev Genet. 2018;19(6):329–46. https://doi.org/10.1038/s41576-018-0003-4. https://www.nature.com/articles/s41576-018-0003-4. Nature Publishing Group.
20. Ren J, et al. lra: A long read aligner for sequences and contigs. PLoS Comput Biol. 2021;17(6): e1009078. https://doi.org/10.1371/journal.pcbi.1009078. https://journals.plos.org/ploscompbiol/article?id=10.1371/journal.pcbi.1009078. Public Library of Science.
21. Shafin K, et al. Nanopore sequencing and the Shasta toolkit enable efficient de novo assembly of eleven human genomes. Nat Biotechnol. 2020;38(9):1044–53. https://doi.org/10.1038/s41587-020-0503-6. https://www.nature.com/articles/s41587-020-0503-6. Nature Publishing Group.
22. Li H. Minimap2: pairwise alignment for nucleotide sequences. Bioinformatics. 2018;34(18):3094–100. https://doi.org/10.1093/bioinformatics/bty191.
23. Sedlazeck FJ, et al. Accurate detection of complex structural variations using single-molecule sequencing. Nat Methods. 2018;15(6):461–8. https://doi.org/10.1038/s41592-018-0001-7.
24. Koren S, et al. Canu: scalable and accurate long-read assembly via adaptive k-mer weighting and repeat separation. Genome Res. 2017;27(5):722–36. https://doi.org/10.1101/gr.215087.116. https://www.ncbi.nlm.nih.gov/pubmed/28298431.
25. Günther T, et al. The presence and impact of reference bias on population genomic studies of prehistoric human populations. PLoS Genet. 2019;15(7): e1008302. https://doi.org/10.1371/journal.pgen.1008302. https://journals.plos.org/plosgenetics/article?id=10.1371/journal.pgen.1008302. Public Library of Science.
26. Asalone KC, et al. Regional sequence expansion or collapse in heterozygous genome assemblies. PLoS Comput Biol. 2020;16(7): e1008104. https://doi.org/10.1371/journal.pcbi.1008104. https://journals.plos.org/ploscompbiol/article?id=10.1371/journal.pcbi.1008104. Public Library of Science
27. Kolmogorov M, et al. Assembly of long, error-prone reads using repeat graphs. Nat Biotechnol. 2019;37(5):540–6. https://doi.org/10.1038/s41587-019-0072-8. https://www.nature.com/articles/s41587-019-0072-8. Nature Publishing Group
28. Garg S, et al. Chromosome-scale, haplotype-resolved assembly of human genomes. Nat Biotechnol. 2021;39(3):309–12. https://doi.org/10.1038/s41587-020-0711-0. https://www.nature.com/articles/s41587-020-0711-0. Nature Publishing Group
29. Weissensteiner MH, et al. Discovery and population genomics of structural variation in a songbird genus. Nat Commun. 2020;11(1):3403. https://doi.org/10.1038/s41467-020-17195-4. https://www.nature.com/articles/s41467-020-17195-4. Nature Publishing Group
30. Jain C, et al. Long-read mapping to repetitive reference sequences using Winnowmap2. Nat Methods. 2022;19(6):705–10. https://doi.org/10.1038/s41592-022-01457-8. https://www.nature.com/articles/s41592-022-01457-8. Nature Publishing Group
31. Overholt WA, et al. Inclusion of Oxford Nanopore long reads improves all microbial and viral metagenome-assembled genomes from a complex aquifer system. Environ Microbiol. 2020;22(9):4000–13. https://doi.org/10.1111/1462-2920.15186.
32. Cheng H, et al. Haplotype-resolved de novo assembly using phased assembly graphs with hifiasm. Nat Methods. 2021;18(2):170–5. https://doi.org/10.1038/s41592-020-01056-5. https://www.nature.com/articles/s41592-020-01056-5. Nature Publishing Group
33. Shafin K, et al. Haplotype-aware variant calling with PEPPER-Margin-DeepVariant enables high accuracy in nanopore long-reads. Nat Methods. 2021;18(11):1322–32. https://doi.org/10.1038/s41592-021-01299-w. https://www.nature.com/articles/s41592-021-01299-w. Nature Publishing Group
34. Nurk S, et al. HiCanu: accurate assembly of segmental duplications, satellites, and allelic variants from high-fidelity long reads. Genome Research. 2020;30(9):1291–305. https://doi.org/10.1101/gr.263566.120. Cold Spring Harbor Lab.
35. Kolmogorov M, et al. metaFlye: scalable long-read metagenome assembly using repeat graphs. Nat Methods. 2020;17(11):1103–10. https://doi.org/10.1038/s41592-020-00971-x. https://www.nature.com/articles/s41592-020-00971-x. Nature Publishing Group
36. Poplin R, et al. A universal SNP and small-indel variant caller using deep neural networks. Nat Biotechnol. 2018;36(10):983–7. https://doi.org/10.1038/nbt.4235. https://www.nature.com/articles/nbt.4235. Nature Publishing Group

37. Zook JM, et al. Extensive sequencing of seven human genomes to characterize benchmark reference materials. Sci Data. 2016;3(1): 160025. https://doi.org/10.1038/sdata.2016.25. https://www.nature.com/articles/sdata201625
38. Zook JM, et al. A robust benchmark for detection of germline large deletions and insertions. Nat Biotechnol. 2020;38(11):1347–55. https://doi.org/10.1038/s41587-020-0538-8. https://www.nature.com/articles/s41587-020-0538-8
39. Nattestad M, et al. Complex rearrangements and oncogene amplifications revealed by long-read DNA and RNA sequencing of a breast cancer cell line. Genome Res. 2018;28(8):1126–35. https://doi.org/10.1101/gr.231100.117. https://genome.cshlp.org/content/28/8/1126
40. Heller D, et al. SVIM: structural variant identification using mapped long reads. Bioinformatics. 2019;35(17):2907–15 https://doi.org/10.1093/bioinformatics/btz041.
41. Jiang T, et al. Long-read-based human genomic structural variation detection with cuteSV. Genome Biol. 2020;21(1):189. https://doi.org/10.1186/s13059-020-02107-y. https://genomebiology.biomedcentral.com/articles/10.1186/s13059-020-02107-y
42. Frické M. Measuring recall. Journal of Information Science. 1998;24(6):409–17. https://doi.org/10.1177/016555159802400604. SAGE Publications Ltd.
43. English AC, et al. Truvari: refined structural variant comparison preserves allelic diversity. Genome Biol. 2022;23(1):271. https://doi.org/10.1186/s13059-022-02840-6.
44. Ho SS, et al. Structural variation in the sequencing era. Nat Rev Genet. 2020;21(3):171–89. https://doi.org/10.1038/s41576-019-0180-9. https://www.nature.com/articles/s41576-019-0180-9. Nature Publishing Group
45. Yang C, et al. NanoSim: nanopore sequence read simulator based on statistical characterization. GigaScience. 2017;6(4):gix010. https://doi.org/10.1093/gigascience/gix010.
46. Li H, et al. A synthetic-diploid benchmark for accurate variant-calling evaluation. Nat Methods. 2018;15(8):595–597. Nature Publishing Group. https://doi.org/10.1038/s41592-018-0054-7. https://www.nature.com/articles/s41592-018-0054-7.
47. Heller D, et al. SVIM-asm: structural variant detection from haploid and diploid genome assemblies. Bioinformatics. 2021;36(22–23):5519–21. https://doi.org/10.1093/bioinformatics/btaa1034. https://academic.oup.com/bioinformatics/article/36/22-23/5519/6042701
48. Pan C, et al. A simple refined DNA minimizer operator enables twofold faster computation. Bioinformatics. 2024;40(2):btae045. https://doi.org/10.1093/bioinformatics/btae045.
49. Berger JO, et al. The likelihood principle. Lect Notes-Monogr Ser. 1988;6:iii–v+vii– xii+1–199. http://www.jstor.org/stable/4355509.
50. Pan C. Leaf: an ultrafast filter for population-scale long-read SV detection: source. 2024. https://doi.org/10.5281/zenodo.11399444. https://zenodo.org/uploads/11399444.
51. Pan C. Leaf: an ultrafast filter for population-scale long-read SV detection: dataset 2. 2024. https://doi.org/10.5281/zenodo.11398751. https://zenodo.org/uploads/11398751.
52. Liao WW, et al. A draft human pangenome reference. Nature. 2023;617(7960):312–24. https://doi.org/10.1038/s41586-023-05896-x. https://www.nature.com/articles/s41586-023-05896-x. Nature Publishing Group
53. Porubsky D, et al. Fully phased human genome assembly without parental data using single-cell strand sequencing and long reads. Nat Biotechnol. 2021;39(3):302–8. https://doi.org/10.1038/s41587-020-0719-5. https://www.nature.com/articles/s41587-020-0719-5. Nature Publishing Group

Publisher's Note